CALPHAD: Computer Coupling of Phase Diagrams and Thermochemistry 33 (2009) 631–641

Contents lists available at ScienceDirect

CALPHAD: Computer Coupling of Phase Diagrams and Thermochemistry

journal homepage: www.elsevier.com/locate/calphad

Solution-based thermodynamic modeling of the Ni–Ta and Ni–Mo–Ta systems using first-principle calculations

S.H. Zhou [a,b], Y. Wang [a], L.-Q. Chen [a], Z.-K. Liu [a], R.E. Napolitano [b,c,*]

[a] Department of Materials Science and Engineering, The Pennsylvania State University, University Park, PA 16802, USA
[b] Materials Sciences, Ames Laboratory, USDOE, USA
[c] Department of Materials Science and Engineering, Iowa State University, USA

ARTICLE INFO

Article history:
Received 24 November 2008
Received in revised form
29 June 2009
Accepted 30 June 2009
Available online 5 August 2009

Keywords:
Alloy thermodynamics
Calphad modeling
Ni-based alloys
Phase diagrams

ABSTRACT

Solution-based thermodynamic descriptions of the Ni–Ta and Ni–Mo–Ta systems are developed with supporting first-principles calculations and reported experimental data for parameter evaluation. For the Ni–Ta system, the liquid, bcc and fcc phases are described with a random solution model, $D0_{22}$–Ni_3Ta is treated as a stoichiometric compound, and the remaining compounds are modeled as solid solutions on multiple sublattices. The resulting model for the Ni–Ta system is integrated with reported treatments of the Ni–Mo and Mo–Ta systems, and a thermodynamic model for the ternary Ni–Mo–Ta system is developed. The zero-Kelvin enthalpies of formation for the intermetallic compounds in the Ni–Mo–Ta system and the enthalpies of mixing for the bcc and fcc special quasirandom structures (SQS) in the binary Ni–Ta system are computed using the Vienna Ab-initio Simulation Package (VASP). Phase equilibria modeling results for the ternary Ni–Mo–Ta system are summarily presented in the form of isothermal sections and liquidus projections, with appropriate comparisons with available experimental data.

1. Introduction

High temperature performance is a critical issue for power generation and transportation applications of Ni-based superalloys, and considerable effort has been devoted to the development of the thermodynamic models required to describe phase stability at elevated temperatures in these materials [1–9]. Specifically, it is necessary to understand the thermodynamic effects of alloying elements, such as Ta and Mo, which play an important role in strategies for increasing the high temperature stability of γ/γ' microstructures. To this end, we focus here on the development of reliable thermodynamic models for the Ni–Ta and Ni–Ta–Mo alloy systems.

Thermodynamic modeling of the Ni–Ta binary system was reported by Kaufman [4] and by Ansara and Selleby [5]. In each of these approaches, a total of eight phases were considered. The liquid, fcc, and bcc phases were treated as single-sublattice solutions, while the C16-$NiTa_2$, μ-NiTa, C11$_b$-Ni_2Ta, κ-Ni_3Ta, and ζ-Ni_8Ta phases were treated as stoichiometric compounds. Subsequently, in order to model the solubility ranges exhibited by certain intermetallic phases, Cui and Jin (CJ) [6] described the κ-Ni_3Ta and C16-$NiTa_2$ phases with two-sublattices and the μ-NiTa phase with four-sublattices. Pan and Jin (PJ) [7] further refined the model by adding a two-sublattice treatment for the C11$_b$-Ni_2Ta phase and reassessing the system, reducing the total number of thermodynamic parameters. The Ni–Ta binary phase diagrams associated with these modeling efforts are shown in Fig. 1, along with relevant experimental data [6,7,10–16]. In addition, Figs. 2 and 3 show that the calculated enthalpy of formation for the compounds at 298 K and enthalpy of mixing for liquid at 1873 K using both the CJ [6] and PJ [7] models differ substantially from reported measurements.

For the Ni–Mo–Ta ternary system, CJ also reported [9] an assessment based on the binary model parameters for the Ni–Mo [9], Mo–Ta [9], and Ni–Ta [6] systems. In their treatment, they model the $D0_a$-Ni_3Mo and κ-Ni_3Ta phases as a single phase. While this approach is reasonable since the two structures differ only in layer packing sequence, the phases are clearly distinct, and we treat them separately here. In addition, the present model incorporates a more recent description of the Ni–Mo system [8] as shown in Fig. 1(d) and a new assessment of the Ni–Ta binary. In subsequent sections of this paper, we will discuss these differences further and present the refined model, which offers better agreement with the experiment.

In the present work, the thermodynamic properties of the Ni–Ta and Ni–Mo–Ta systems and the associated phase equilibria are

* Corresponding author at: Materials Sciences, Ames Laboratory, USDOE, USA. Tel.: +1 515 294 9101; fax: +1 515 294 9101.
E-mail address: ralphn@iastate.edu (R.E. Napolitano).

0364-5916/$ – see front matter © 2009 Elsevier Ltd. All rights reserved.
doi:10.1016/j.calphad.2009.06.006

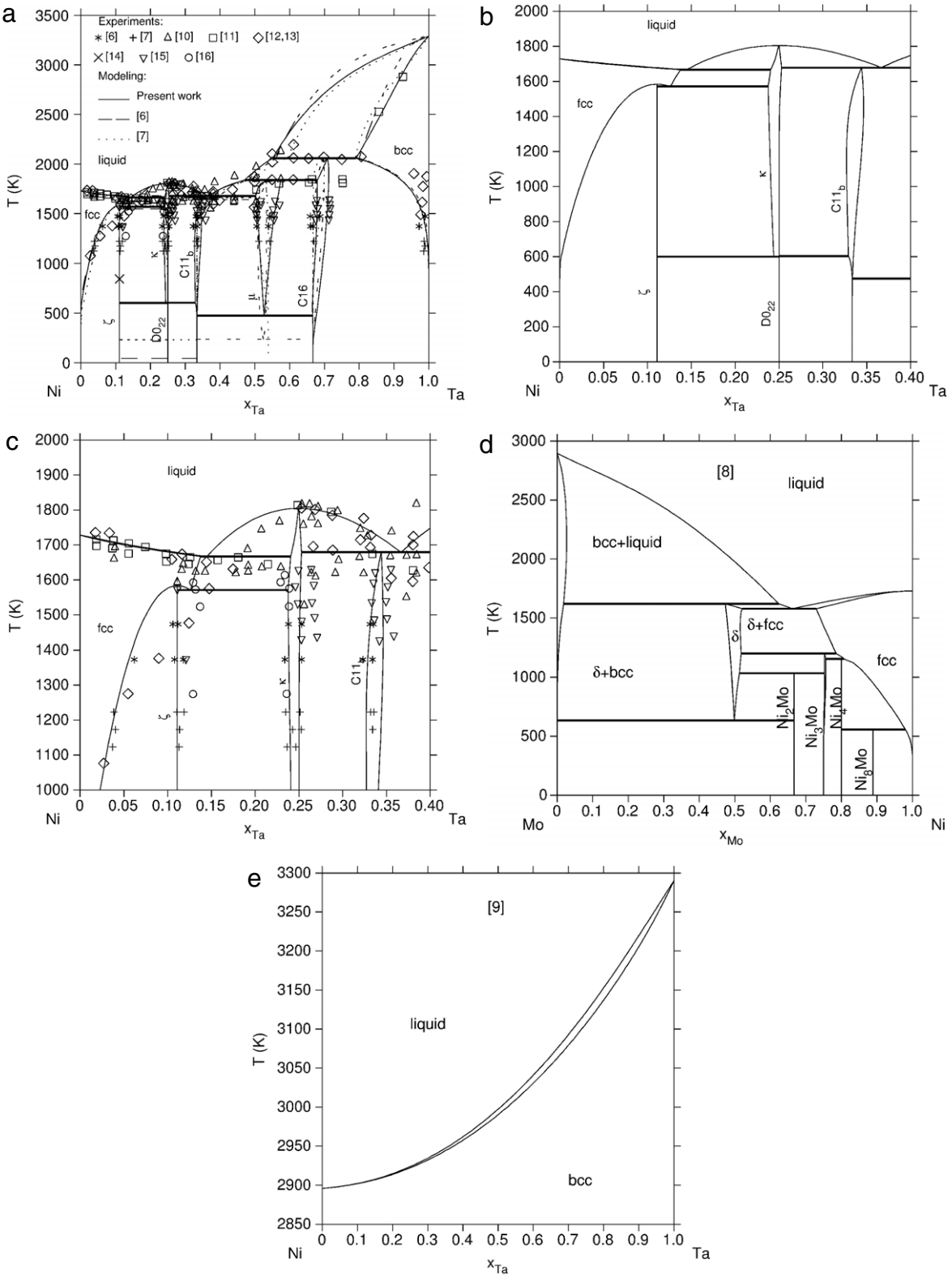

Fig. 1. The Ni–Ta phase diagram computed from the current model (a) shown over the full range of composition, compared with previous models and reported experimental data and shown over the Ni-rich portion of the binary range, without (b) and with (c) relevant experimental data. The Ni–Mo and Mo–Ta phase diagram plotted in (d) and (e) respectively.

described by incorporating the first-principles calculations into a general CALPHAD [17,18] approach. The evaluation starts with the binary Ni–Ta system, for which the thermodynamic parameters are evaluated with the first-principles calculated enthalpies of formation and all available experimental data [6,7,10–16,19–22]. Special quasirandom structures (SQS) [23,24] are used to calculate the enthalpies of mixing for the bcc and fcc phases from first-principles, and the results are incorporated into the comprehensive model.

For the ternary Ni–Mo–Ta system, a distinguishing feature of our approach, in comparison with that reported in Ref [9], is

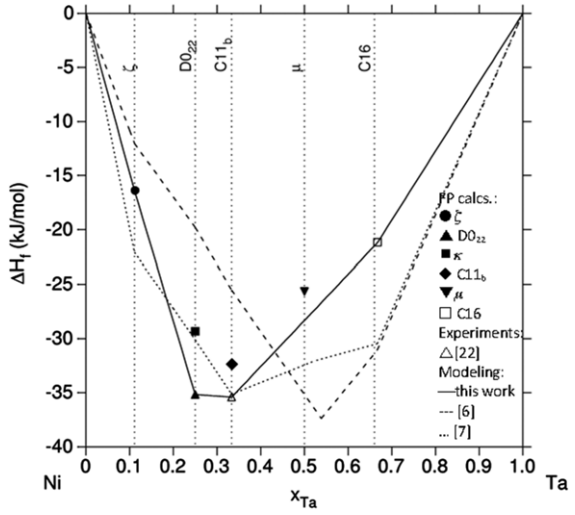

Fig. 2. The enthalpy of formation of the Ni–Ta system, as computed using the present model, shown with first-principles calculations and reported experimental data.

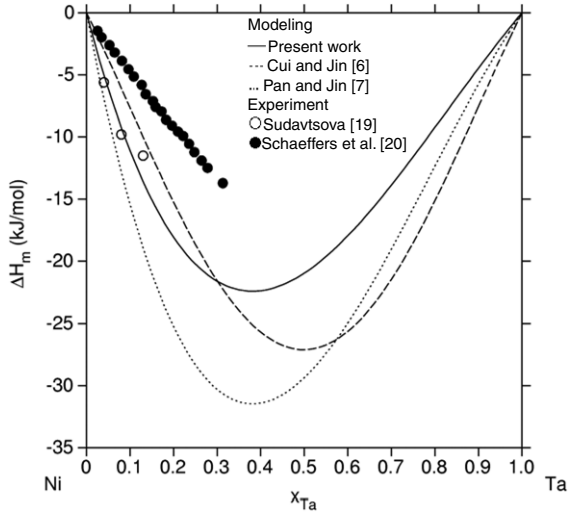

Fig. 3. The enthalpy of mixing in liquid at 1873 K, as computed using the present model. Reported experimental data and prior modeling are also shown.

that we allow for Mo–Ta substitution. For example, the stable $D0_a$-Ni_3Mo and metastable $D0_a$-Ni_3Ta phases (Cu_3Ti structure [25,26]) are treated as a single solution phase denoted by $D0_a$-Ni_3(Mo, Ta). Similarly, the metastable κ-Ni_3Mo and stable κ-Ni_3Ta phases (Pt_3Ta structure [25,26]) are described as κ-Ni_3(Mo, Ta), and the stable Ni_8Ta and Ni_8Mo phases (Ni_8Nb structure [14]) are described as ζ-Ni_8(Mo, Ta). The ternary parameters for the individual phases are evaluated using all available experimental information [9,27–29], and the resulting model for phase equilibria in this ternary system are presented in the forms of liquidus projections and isothermal sections of the phase diagram.

2. Thermodynamic models

The phases considered in the present model are listed in Table 1, indicating the symbol to be used in this paper and the prototype structure. The thermodynamic properties of pure Ni, Mo, and Ta in the various relevant structures are computed using the parameters from the SGTE database [30], as listed in Table 2. In addition to the compounds in the Ni–Mo system described in Ref. [8], the fcc, bcc and liquid phases are modeled as simple ternary

Table 1
A listing of phases modeled in the current treatment.

Formula unit	Sym.	Lattice	Struk. Des.	Prototype	Ref.
Phases extending from the pure component states:					
Ni, Ta, Mo	–	–	–	Liquid	–
Ni	–	cub	A1	fcc	–
Ta	–	cub	A2	bcc	–
Mo	–	cub	A2	bcc	–
Phases extending from the Ni–Ta binary system:					
$NiTa_2$	–	tet	C16	Al_2Cu	[33]
NiTa	μ	trig	$D8_5$	Fe_7W_6	[33]
Ni_2Ta	–	tet	$C11_b$	$MoSi_2$	[25,26]
Ni_3Ta	κ	mono	–	Pt_3Ta	[25,26]
	–	tet	$D0_{22}$	Al_3Ti	[25,26]
Ni_8Ta	ζ	tet	–	Ni_8Nb	[14]
Phases extending from the Ni–Mo binary system:					
NiMo	δ	orth	–	NiMo	[25]
Ni_2Mo	–	tet	–	Pt_2Mo	[34]
Ni_3Mo	–	tet	$D0_a$	Cu_3Ti	[25]
Ni_4Mo	–	tet	$D1_a$	Ni_4Mo	[25]
Ni_8Mo	ζ	tet	–	Ni_8Nb	[14]

substitutional solutions, the C16-$NiTa_2$, μ-NiTa, $C11_b$-Ni_2Ta, κ-Ni_3 (Mo, Ta), $D0_a$-Ni_3(Mo, Ta) and ζ-Ni_8(Mo, Ta) intermetallic phases are described with a sublattice formalism [31], while the $D0_{22}$-Ni_3Ta phase is treated as stoicheometric compound in the ternary Ni–Mo–Ta system. The thermodynamic models are defined in Table 3, where the total Gibbs free energy for any phase, Φ, is generally given by the sum of three contributions,

$$G_m^{\Phi} = {}^{ref}G_m^{\Phi} + {}^{id}G_m^{\Phi} + {}^{xs}G_m^{\Phi}, \tag{1}$$

where the subscript m denote that all terms are molar quantities of formular unit. The first term in Eq. (1) is given by the sum of occupancy-weighted sublattice end-member contributions. The second and third terms are the ideal and excess parts of the Gibbs free energy of mixing, respectively. In Table 3, a Redlich–Kister polynomial [32] is used to describe the composition and temperature dependence of the excess Gibbs free energy associated with mixing. The specific treatment of each phase is discussed briefly here.

The liquid, fcc and bcc phases are described with a single lattice, using the model given in Table 3, where ${}^0G_i^{\Phi}$ is the molar Gibbs free energy of the pure element i with the structure Φ (Φ = liquid, fcc or bcc), as listed in Table 2, and x_i is the mole fraction of the indicated component i. ${}^jL_{i,k}^{\Phi}$ is the binary interaction parameter, and $L_{Mo,Ni,Ta}^{\Phi}$ is a composition dependent ternary interaction parameter, expressed as $L_{Mo,Ni,Ta}^{\Phi} = x_{Mo}\,{}^0L_{Mo,Ni,Ta}^{\Phi} + x_{Ni}\,{}^1L_{Mo,Ni,Ta}^{\Phi} + x_{Ta}\,{}^2L_{Mo,Ni,Ta}^{\Phi}$, where the parameters ${}^0L_{Mo,Ni,Ta}^{\Phi}$, ${}^1L_{Mo,Ni,Ta}^{\Phi}$ and ${}^2L_{Mo,Ni,Ta}^{\Phi}$ may be temperature dependent and are evaluated with experimental data.

The μ-NiTa phase has been reported [33] to have a rhombohedral structure (Fe_7W_6 prototype) with a primitive unit cell of 13 atoms, distributed in five sublattices as $(Ni, Ta)_1^{12}(Ta)_2^{15}(Ta)_2^{16}(Ni, Ta)_2^{14}(Ni, Ta)_6^{12}$. (The subscript is the number of sites in that sublattice, and the superscript is the coordination number.) The analysis by Andersson et al. [35], later showed that fcc and bcc elements prefer sublattices with a coordination numbers of 12 while bcc elements prefer sublattices with coordination numbers of 14 and 15. This led to the use of a four-sublattice model by Ansara et al. [36] and was supported by the investigation of Joubert and Dupin [37], where the atom distribution was confirmed to be $(Ni, Ta)_1(Ta)_4(Ni, Ta)_2(Ni, Ta)_6$, which we adopt here. The corresponding Gibbs free energy terms are given in Table 3, where y^{I}, y^{III}, and y^{IV} are the site occupancy fractions in the first, third and fourth sublattices, respectively. ${}^kL^{\mu}$ is the kth interaction parameter, expressed as ${}^ka^{\mu} + {}^kb^{\mu}T$. ${}^0G_{i:Ta:j:k}^{\mu}$ represents the Gibbs free energy of the end-members $(i)_1(Ta)_4(j)_2(k)_6$ with the Gibbs free energy of formation, $\Delta G_{i:Ta:j:k}^{\mu}$, being expressed as $a_{i:Ta:j:k}^{\mu} + b_{i:Ta:j:k}^{\mu}T$. Considering the composition range of μ-NiTa phase being around 0.5, the

Table 2
The thermodynamic parameters for pure elements [30].

Mo phases					
	${}^0G^{liq}_{Mo}$		${}^0G^{bcc}_{Mo}$		${}^0G^{fcc}_{Mo}$
T_{min}	298	2896	298	2896	298
T_{max}	2896	5000	2896	3200	5000
${}^0G^{ref}$	${}^0G^{bcc}_{Mo}$	–	–	–	${}^0G^{bcc}_{Mo}$
a_0	41831.347	3538.963	−7746.302	−30556.41	15200
a_1	−14.694912	271.6697	131.9197	283.559746	0.63
a_2	–	−42.63829	−23.56414	−42.63829	–
a_3	–	–	−0.003443396	–	–
a_4	–	–	5.66283×10^{-7}	–	–
a_5	–	–	-1.30927×10^{-10}	–	–
a_6	–	–	65812.39	–	–
a_7	–	–	–	-4.849315×10^{33}	–
a_8	4.24519×10^{-22}	–	–	–	–
Ni phases					
	${}^0G^{liq}_{Ni}$		${}^0G^{bcc}_{Ni}$	${}^0G^{fcc}_{Ni}$	
T_{min}	298	1728	298	298	1728
T_{max}	1728	6000	6000	1728	6000
${}^0G^{ref}$	${}^0G^{fcc}_{Ni}$	–	${}^0G^{fcc}_{Ni}$	–	–
a_0	16414.686	−9549.775	8715.084	−5179.159	−27840.655
a_1	−9.397	268.598	−3.556	117.854	279.135
a_2	–	−43.1	–	−22.096	−43.1
a_3	–	–	–	−0.0048407	–
a_4	–	–	–	–	–
a_5	–	–	–	–	–
a_6	–	–	–	–	–
a_7	–	–	–	–	1.12754×10^{31}
a_8	-3.82318×10^{-21}	–	–	–	–
T_c	–	–	575	633	–
β	–	–	0.85	0.52	–
Ta phases					
	${}^0G^{liq}_{Ta}$		${}^0G^{fcc}_{Ta}$	${}^0G^{bcc}_{Ta}$	
T_{min}, K	298	3290	298	298	1300	2500	3290
T_{max},K	3290	6000	6000	1300	2500	3290	6000
${}^0G^{ref}$	${}^0G^{bcc}_{Ta}$	–	${}^0G^{bcc}_{Ta}$	–	–	–	–
a_0	29160.975	43884.339	16000	−7285.889	−22389.955	229382.886	−1042384.01
a_1	−7.578729	−61.981795	1.7	119.139857	243.88676	−722.59722	2985.49125
a_2	–	0.0279523	–	−23.7592624	−41.137088	78.5244752	−362.159132
a_3	–	−0.01233	–	−0.002623033	0.00616757	−0.0179833	0.043117795
a_4	–	6.1459×10^{-7}	–	1.70109×10^{-7}	-6.551×10^{-7}	1.9503×10^{-7}	-1.055148×10^{-6}
a_5	–	–	–	–	–	–	–
a_6	–	−3523338	–	−3293	2429586	−93813648	5.54714342×10^{8}
a_7	–	–	–	–	–	–	–
a_8	–	–	–	–	–	–	–

Note: ${}^0G^{\phi}_i = a_0 + a_1T + a_2T\ln T + a_3T^2 + a_4T^3 + a_5T^4 + a_6T^{-1} + a_7T^{-9} + a_8T^7$ and T_c (K) is the Curie temperature and β is the average magnetic moment per atom (Bohr magnetons).

parameters $\Delta G^{\mu}_{Ni:Ta:Ta:Ni}$ (at Ni_7Ta_6) and $\Delta G^{\mu}_{Ta:Ta:Ta:Ni}$ (at Ni_6Ta_7) are selected first. These two parameters, however, are not sufficient to describe the composition range of the μ-NiTa phase. To extend the composition range to left side, the parameter $\Delta G^{\mu}_{Ta:Ta:Ta:Ta}$ as well as the associated interaction parameter ${}^0L^{\mu}_{Ta:Ta:Ta:Ni,Ta}$ between end members $Ta_1Ta_4Ta_2Ni_6$ and $Ta_1Ta_4Ta_2Ta_6$ is included. Using the same arguments, the parameters $\Delta G^{\mu}_{Ni:Ta:Ni:Ni}$, $\Delta G^{\mu}_{Ta:Ta:Ni:Ni}$, and ${}^0L^{\mu}_{Ta:Ta:Ni,Ta:Ni}$ are employed to extend composition range to right side. To accommodate the small solubility of Mo in the μ-NiTa phase in ternary system, we modify this formulation to $(Ni, Ta)_1(Ta)_4(Mo, Ni, Ta)_2(Ni, Ta)_6$, permitting Mo on the third sublattice, and introduce the ternary parameters $\Delta G^{\mu}_{Ta:Ta:Mo:Ni}$ and ${}^0L^{\mu}_{Ta:Ta:Mo,Ta:Ni}$. These parameters are sufficient for describing the μ-NiTa phase, and the contributions from the remaining end members (i.e $G^{\mu}_{Ni:Ta:Ta:Ta}$, $G^{\mu}_{Ta:Ta:Ni:Ta}$, $G^{\mu}_{Ni:Ta:Ni:Ta}$, $G^{\mu}_{Ta:Ta:Mo:Ta}$, $G^{\mu}_{Ni:Ta:Mo:Ni}$, and $G^{\mu}_{Ni:Ta:Mo:Ta}$) listed in Table 3 are assumed to be zero.

The atoms in the κ-$Ni_3(Mo, Ta)$, C16-$NiTa_2$ and C11$_b$-Ni_2Ta phases are distributed in two sublattices. The experimental data [6,7,10–12,15,16,28] reveal a homogeneous composition range for these phases, and each is described here with a two-sublattice model, as shown in Table 3, where $a^{\Phi}_{i:j}$, $b^{\Phi}_{i:j}$, ${}^0L^{\Phi}_{i,l:j}$ and ${}^0L^{\Phi}_{j:i,l}$ are the parameters to be evaluated.

Due to a lack of experimental data for D0$_{22}$-Ni_3Ta, ζ-Ni_8Ta, and ζ-Ni_8Mo, these phases are treated as stoichiometric compounds in their respective binary systems. In the ternary Ni–Mo–Ta system, the experimental investigations by Chakravortye et al. [28] indicated a small solubility of Mo in ζ-Ni_8Ta. Accordingly, the ζ-Ni_8Ta and ζ-Ni_8Mo phases are described here using a $(Ni)_8(Mo, Ta)$ formulation, and the corresponding Gibbs free energy function is given in Table 3.

The D0$_a$-Ni_3Mo and δ-NiMo phases are treated with a three-sublattice model using the formulation $(Mo, Ni)_4(Ni)_2(Mo, Ni)_2$ and $(Ni)_{24}(Mo, Ni)_{20}(Mo)_{12}$ as described in Ref. [8]. The experimental data by Chakravorty and West [28] and Cui et al. [9] revealed a small solubility of Ta in D0$_a$-Ni_3Mo and δ-NiMo. These phases, denoted by D0$_a$-$Ni_3(Mo, Ta)$ and δ-NiMo, are modeled here by considering the substitution of Ta for Mo, i.e. $(Mo, Ni, Ta)_4(Ni)_2(Mo, Ni, Ta)_2$ and $(Ni)_{24}(Mo, Ni, Ta)_{20}(Mo, Ta)_{12}$, respectively, with the Gibbs free energy functions given in

Table 3
Summary of the thermodynamic models used for the Ni–Mo–Ta ternary system with the total Gibbs free energy $G_m^{\Phi} = {}^{ref}G_m^{\Phi} + {}^{id}G_m^{\Phi} + {}^{xs}G_m^{\Phi}$.

Phase	Sublattice formulation	Model
Liquid fcc (A1) bcc (A2)	$(Mo, Ni, Ta)_1$	${}^{ref}G_m^{\Phi} = x_{Ni}{}^0G_{Ni}^{\Phi} + x_{Mo}^0G_{Mo}^{\Phi} + x_{Ta}^0G_{Ta}^{\Phi}$ ${}^{id}G_m^{\Phi} = RT(x_{Ni}\ln x_{Ni} + x_{Mo}\ln x_{Mo} + x_{Ta}\ln x_{Ta})$ ${}^{xs}G_m^{\Phi} = x_{Mo}x_{Ni}\sum_{j=0}^{n}{}^jL_{Mo,Ni}^{\Phi}(x_{Mo}-x_{Ni})^j + x_{Mo}x_{Ta}\sum_{j=0}^{n}{}^jL_{Mo,Ta}^{\Phi}(x_{Mo}-x_{Ta})^j$ $+ x_{Ni}x_{Ta}\sum_{j=0}^{n}{}^jL_{Ni,Ta}^{\Phi}(x_{Ni}-x_{Ta})^j + x_{Mo}x_{Ni}x_{Ta}L_{Mo,Ni,Ta}^{\Phi}$
μ	$(Ni, Ta)_1(Ta)_4(Mo, Ni, Ta)_2(Ni, Ta)_6$ Reference States: Group 1: Ni:Ta:Ni:Ni Ni:Ta:Ta:Ni Ta:Ta:Ni:Ni Ta:Ta:Ta:Ni Ta:Ta:Ta:Ta Ta:Ta:Mo:Ni Group 2: Ni:Ta:Ta:Ta Ta:Ta:Ni:Ta Ni:Ta:Ni:Ta Ta:Ta:Mo:Ta Ni:Ta:Mo:Ni Ni:Ta:Mo:Ta	${}^{ref}G_m^{\mu} = \sum_{i=Ni,Ta}y_i^{I}\sum_{j=Mo,Ni,Ta}y_j^{III}\sum_{k=Ni,Ta}y_k^{IV}{}^0G_{i:Ta:j:k}^{\mu}$ ${}^0G_{i:Ta:j:k}^{\mu} = {}^0G_i^{fcc} + 4{}^0G_{Ta}^{bcc} + 2{}^0G_j^{bcc} + 6{}^0G_k^{fcc} + \Delta G_{i:Ta:j:k}^{\mu}(Group\ 1)$ ${}^0G_{i:Ta:j:k}^{\mu} = 0(Group\ 2)$ ${}^{id}G_m^{\mu} = RT\left(\sum_{i=Ni,Ta}(y_i^{I}\ln y_i^{I} + 2y_i^{III}\ln y_i^{III} + 6y_i^{IV}\ln y_i^{IV})\right)$ ${}^{xs}G_m^{\mu} = y_{Ni}^{I}y_{Ta}^{I}\sum_{i=Mo,Ni,Ta}\sum_{j=Ni,Ta}\sum_{k=0}{}^kL_{Ni,Ta:Ta:i:j}^{\mu}(y_{Ni}^{I}-y_{Ta}^{I})^k$ $+ \sum_{l=Mo,Ni}\sum_{p=Ni,Ta}y_l^{III}y_p^{III}\sum_{i=Ni,Ta}\sum_{j=Ni,Ta}\sum_{k=0}{}^kL_{i:Ta:l,p:j}^{\mu}(y_l^{III}-y_p^{III})^k$ $+ y_{Ni}^{IV}y_{Ta}^{IV}\sum_{i=Ni,Ta}\sum_{j=Mo,Ni,Ta}\sum_{k=0}{}^kL_{i:Ta:j:Ni,Ta}^{\mu}(y_{Ni}^{IV}-y_{Ta}^{IV})^k$
$D0_aI$	$(Mo, Ni, Ta)_4(Ni)_2(Mo, Ni, Ta)_2$ Reference states: Group 1: Mo:Ni:Mo Ni:Ni:Mo Ta:Ni:Ta Ni:Ni:Ta Ni:Ni:Ni Group 2: (Mo, Ta):Ni:Ni Mo:Ni:Ta Ta:Ni:Mo	${}^{ref}G_m^{D0_a} = \sum_{i=Mo,Ni,Ta}y_i^{I}\sum_{j=Mo,Ni,Ta}y_j^{III}{}^0G_{i:Ni:j}^{D0_a}$ ${}^0G_{i:Ni:j}^{D0_a} = 4{}^0G_i^{fcc} + 2{}^0G_{Ni}^{fcc} + 2{}^0G_j^{fcc} + \Delta G_{i:Ni:j}^{D0_a}(Group\ 1)$ ${}^0G_{i:Ni:j}^{D0_a} = (Group\ 2)$ ${}^{id}G_m^{D0_a} = RT\sum_{i=Mo,Ni,Ta}(4y_i^{I}\ln y_i^{I} + 2_i^{III}\ln y_i^{III})$ ${}^{xs}G_m^{D0_a} = \sum_i\sum_{k>i}y_i^{I}y_k^{I}\sum_j\sum_{n=0}{}^nL_{i,k:Ni:j}^{D0_a}(y_i^{I}-y_k^{I})^n$ $+ \sum_j\sum_i\sum_{k>i}y_i^{III}y_k^{III}\sum_{n=0}L_{i:Ni:i,k}^{D0_a}(y_i^{III}-y_k^{III})^n$
κ $D0_aII$	$(Ni, Mo, Ta)_3(Ni, Mo, Ta)_1$ Note: ${}^0G_{Mo:Ta}^{D0_aII} = {}^0G_{Ta:Mo}^{D0_aII} = 0$	${}^{ref}G_m^{\Phi} = \sum_{i=Mo,Ni,Ta}y_i^{I}\sum_{j=Mo,Ni,Ta}y_j^{II}{}^0G_{i:j}^{\Phi}$ ${}^0G_{i:j}^{\Phi} = p^0G_i^{ref} + q^0G_j^{ref} + \Delta G_{i:j}^{\Phi} = p^0G_i^{ref} + q^0G_j^{ref} + a_{i:j}^{\Phi} + b_{i:j}^{\Phi}T$ ${}^{id}G_m^{\Phi} = RT\sum_{i=Mo,Ni,Ta}(py_i^{I}\ln y_i^{I} + qy_i^{II}\ln y_i^{II})$ ${}^{xs}G_m^{\Phi} = \sum_i\sum_{l>i}y_i^{I}y_l^{I}\sum_j\sum_{k=0}{}^kL_{i,l:j}^{\Phi}(y_i^{I}-y_l^{I})^k$ $+ \sum_j\sum_i\sum_{l>i}y_i^{II}y_l^{II}\sum_{k=0}{}^kL_{j:i,l}^{\Phi}(y_i^{II}-y_l^{II})^k$ (p and q are the subscript numbers of sublattices, respectively)
C16	$(Ni, Ta)_1(Ni, Ta)_2$	
$C11_b$	$(Ni, Ta)_2(Ni, Ta)_1$	
ζ	$(Ni)_8(Mo, Ta)$	
δ	$(Ni)_{24}(Mo, Ni, Ta)_{20}(Mo, Ta)_{12}$	${}^{ref}G_m^{\mu} = \sum_{i=Mo,Ni,Ta}y_i^{II}\sum_{j=Mo,Ta}y_j^{III}{}^0G_{Ni:i:j}^{\delta}$ ${}^0G_{Ni:i:j}^{\delta} = 24{}^0G_{Ni}^{fcc} + 20{}^0G_i^{bcc} + 12{}^0G_j^{bcc} + \Delta G_{Ni:i:j}^{\delta}$ ${}^{id}G_m^{\delta} = RT\left(\sum_{i=Ni,Ta}(20y_i^{II}\ln y_i^{II} + 12y_i^{III}\ln y_i^{III})\right)$ ${}^{xs}G_m^{\delta} = \sum_{i=Mo,Ni}\sum_{j=Ni,Ta}y_i^{II}y_j^{II}\sum_{l=Mo,Ta}\sum_{k=0}{}^kL_{Ni:i,j:l}^{\delta}(y_i^{II}-y_j^{II})^k$ $+ \sum_{i=Mo,Ni,Ta}y_{Mo}^{III}y_{Ta}^{III}\sum_{k=0}{}^kL_{Ni:i:Mo,Ta}^{\mu}(y_{Mo}^{III}-y_{Ta}^{III})^k$
Ni_2Mo	$(Ni)_2(Mo)_1$	$G_m^{\Phi} = \Delta G_{Ni:Ta}^{\Phi} + p^0G_{Ni}^{fcc} + q^0G_{i(i=Mo,Ta)}^{bcc}$ $= a^{\Phi} + b^{\Phi}T + p^0G_{Ni}^{fcc} + q^0G_{i(i=Mo,Ta)}^{bcc}$ (p and q are the subscript numbers of sublattices, respectively)
Ni_4Mo	$(Ni)_4(Mo)_1$	
$D0_{22}$	$(Ni)_3(Ta)_1$	

Table 3. $D0_a$-Ni_3Mo was also described with the two-sublattice model using the $(Mo, Ni)_3(Mo, Ni)_1$ formulation in Ref. [8]. To be compatible with this treatment in the ternary system, another set of parameters is developed for the two-sublattice model, i.e. $(Mo, Ni, Ta)_3(Mo, Ni, Ta)_1$, denoted by $D0_aII$–$Ni_3(Mo, Ta)$. In this case, the Gibbs free energy functions can be written in the same form as those for κ-$Ni_3(Mo, Ta)$ in Table 3.

3. Determination of the thermodynamic model parameters

In the determination of the model parameters for the ternary Ni–Mo–Ta system, the Ni–Ta binary is evaluated first and then integrated with reported models for the Ni–Mo [8] in Fig. 1(d) and Mo–Ta [9] in Fig. 1(e) systems to build the thermodynamic description. With the thermodynamic models described in the preceding section, we employ a total of twenty-four Gibbs free energy of formation parameters and fourteen interaction parameters for the binary Ni–Ta system, as listed in Tables 4 and 5. The evaluation process, utilizing both experimental data and first principles results for the Ni–Ta system, is discussed in this section.

Using VASP [38] with the Vanderbilt ultrasoft pseudopotential [39] within the generalized gradient approximation (GGA) [40], the total energy of the fcc-Ni, bcc-Mo, bcc-Ta, and compounds are calculated. Monkhorst $15 \times 15 \times 15$ k points are used for the pure elements Ni, Mo and Ta, $11 \times 11 \times 11$ k points for the end-members of the ζ-Ni_8Ta, $D0_{22}$-Ni_3Ta, $C11_b$-Ni_2Ta, $D0_a$-Ni_3Mo and C16-$NiTa_2$ phases, $9 \times 9 \times 9$ k points for the end-members of the μ-NiTa phase and $4 \times 4 \times 4$ k points for the end-members of the κ-Ni_3Ta phase. To ensure that the unit cell corresponds to a stable structure, we fully relax the cell shape and the internal atomic coordinates for the stable end-members and relax only the cell volume for the unstable/metastable end-members.

Table 4
Gibbs free energy of formation for end-member reference states (per mole of formula unit).

Phase	Parameter	Value (J/mol)	Ref.
C16	$\Delta G^{C16}_{Ni:Ni}$	80310	Present
	$\Delta G^{C16}_{Ta:Ni}$	132420	
	$\Delta G^{C16}_{Ni:Ta}$	$-65550 + 6.246T$	
	$\Delta G^{C16}_{Ta:Ta}$	152640	
μ	$\Delta G^{\mu}_{Ni:Ta:Ni:Ni}$	−167960	
	$\Delta G^{\mu}_{Ta:Ta:Ni:Ni}$	−149240	
	$\Delta G^{\mu}_{Ni:Ta:Ta:Ni}$	−298870	
	$\Delta G^{\mu}_{Ta:Ta:Ta:Ni}$	$-356630 + 24.003T$	
	$\Delta G^{\mu}_{Ta:Ta:Ta:Ta}$	221650	
	$\Delta G^{\mu}_{Ta:Ta:Mo:Ni}$	−320230	
$C11_b$	$\Delta G^{C11_b}_{Ni:Ni}$	23730	
	$\Delta G^{C11_b}_{Ta:Ni}$	15000	
	$\Delta G^{C11_b}_{Ni:Ta}$	$-110001 + 20.919T$	
	$\Delta G^{C11_b}_{Ta:Ta}$	31470	
κ	$\Delta G^{\kappa}_{Ni:Ni}$	14000	
	$\Delta G^{\kappa}_{Ni:Ta}$	$-122760 + 11.692T$	
	$\Delta G^{\kappa}_{Ta:Ni}$	50160	
	$\Delta G^{\kappa}_{Ta:Ta}$	117280	
	$\Delta G^{\kappa}_{Ta:Mo}$	128320	
	$\Delta G^{\kappa}_{Mo:Ta}$	146400	
	$\Delta G^{\kappa}_{Mo:Mo}$	164360	
	$\Delta G^{\kappa}_{Ni:Mo}$	$-15440 + 74.112T - 9.82380T\ln(T)$	
	$\Delta G^{\kappa}_{Mo:Ni}$	75400	
$D0_a$-I	$\Delta G^{D0_a}_{Ta:Ni:Ta}$	99840	Present
	$\Delta G^{D0_a}_{Ni:Ni:Ta}$	$-275040 + 74.368T$	Present
	$\Delta G^{D0_a}_{Mo:Ni:Mo}$	136480	[8]
	$\Delta G^{D0_a}_{Ni:Ni:Mo}$	$-81055.2 + 465.054T - 58.929T\ln(T)$	[8]
	$\Delta G^{D0_a}_{Ni:Ni:Ni}$	22720	[8]
$D0_a$-II	$\Delta G^{D0_aII}_{Ta:Ta}$	123200	Present
	$\Delta G^{D0_aII}_{Ni:Ta}$	$\Delta G^{D0_a}_{Ni:Ni:Ta}/2$	Present
	$\Delta G^{D0_aII}_{Ta:Ni}$	$\Delta G^{D0_a}_{Ta:Ni:Ta}/2$	Present
	$\Delta G^{D0_aII}_{Mo:Mo}$	170600	[8]
	$\Delta G^{D0_aII}_{Ni:Mo}$	$\Delta G^{Ni_3Mo}_{Ni:Ni:Mo}/2$	[8]
	$\Delta G^{D0_aII}_{Mo:Ni}$	$\Delta G^{Ni_3Mo}_{Mo:Ni:Mo}/2$	[8]
	$\Delta G^{D0_aII}_{Ni:Ni}$	$\Delta G^{Ni_3Mo}_{Ni:Ni:Ni}/2$	[8]
ζ	$\Delta G^{\zeta}_{Ni:Ta}$	$-162918 + 20.736T$	Present
	$\Delta G^{\zeta}_{Ni:Mo}$	$-55035 + 299.322T - 36.765T\ln(T)$	[8]
δ	$\Delta G^{\delta}_{Ni:Mo:Mo}$	$-169981 + 1154.981T - 155.484T\ln(T)$	[8]
	$\Delta G^{\delta}_{Ni:Ni:Mo}$	$-154106 + 2855.001T - 394.923T\ln(T)$	[8]
	$\Delta G^{\delta}_{Ni:Ta:Mo}$	−1224888	Present
	$\Delta G^{\delta}_{Ni:Mo:Ta}$	−679392	Present
	$\Delta G^{\delta}_{Ni:Ni:Ta}$	−1203776	Present
	$\Delta G^{\delta}_{Ni:Ta:Ta}$	34496	Present
Ni_2Mo	$\Delta G^{Ni_2Mo}_{Ni:Mo}$	$-28263 + 148.653T - 18.693T\ln(T)$	[8]
Ni_4Mo	$\Delta G^{Ni_4Mo}_{Ni:Mo}$	$-45105 + 275.020T - 35.400T\ln(T)$	[8]
$D0_{22}$	$\Delta G^{D0_{22}}_{Ni:Ta}$	$-146360 + 50.804T$	Present

Table 5
Excess Gibbs free energy interaction parameters.

Phase	Parameters	Value (J/mol)	Ref.
Liquid	${}^0L^{liq}_{Ni,Ta}$	−83812	Present
	${}^1L^{liq}_{Ni,Ta}$	−46039	
	${}^2L^{liq}_{Ni,Ta}$	−4023	
	${}^0L^{liq}_{Mo,Ta}$	−73477	[9]
	${}^1L^{liq}_{Mo,Ta}$	−4091	
	${}^0L^{liq}_{Mo,Ni}$	$-39597 + 15.935T$	[8]
	${}^1L^{liq}_{Mo,Ni}$	$-7373 + 4.102T$	
	${}^2L^{liq}_{Mo,Ni}$	$-12123 + 5.551T$	
Bcc	${}^0L^{bcc}_{Ni,Ta}$	$-28415 - 10.613T$	Present
	${}^1L^{bcc}_{Ni,Ta}$	−32471	
	${}^0L^{bcc}_{Mo,Ta}$	−69360	[9]
	${}^1L^{bcc}_{Mo,Ta}$	−4190	
	${}^0L^{bcc}_{Mo,Ni}$	27691	[8]
	${}^1L^{bcc}_{Mo,Ni}$	18792	
	${}^0L^{bcc}_{Mo,Ni,Ta}$	$-140353 + 59.354T$	
	${}^1L^{bcc}_{Mo,Ni,Ta}$	28573	
	${}^2L^{bcc}_{Mo,Ni,Ta}$	$-126245 + 73.235T$	Present
Fcc	${}^0L^{fcc}_{Ni,Ta}$	$-75470 - 4.023T$	
	${}^1L^{fcc}_{Ni,Ta}$	$-71135 + 13.235T$	
	${}^0L^{fcc}_{Mo,Ta}$	−6572	[9]
	${}^0L^{fcc}_{Mo,Ni}$	$-8916 + 3.591T$	[8]
	${}^1L^{fcc}_{Mo,Ni}$	$5469 - 0.249T$	
	${}^2L^{fcc}_{Mo,Ni}$	$-1549 - 2.741T$	
	${}^0L^{fcc}_{Mo,Ni,Ta}$	45410	Present
	${}^1L^{fcc}_{Mo,Ni,Ta}$	$-20214 - 27.435T$	
	${}^2L^{fcc}_{Mo,Ni,Ta}$	−45001	
C16	${}^0L^{C16}_{Ni:Ni,Ta}$	$-190695 + 46.446T$	
	${}^0L^{C16}_{Ni,Ta:Ta}$	$-137991 - 19.629T$	
μ	${}^0L^{\mu}_{Ta:Ta:Ni,Ta:Ni}$	$-377513 + 70.302T$	
	${}^0L^{\mu}_{Ta:Ta:Ta:Ni,Ta}$	$-405208 + 50.923T$	
	${}^0L^{\mu}_{Ta:Ta:Mo,Ta:Ni}$	−71310	
$C11_b$	${}^0L^{C11_b}_{Ni:Ni,Ta}$	−58029	
κ	${}^0L^{\kappa}_{Ni:Ni,Ta}$	$-42372 + 30.436T$	
	${}^0L^{\kappa}_{Ni,Ta:Ta}$	$-42373.6 + 40.516T$	
	${}^0L^{\kappa}_{Mo,Ni:Mo}$	−14045.5	
	${}^0L^{\kappa}_{Ni:Mo,Ta}$	$-32440 + 11.428T$	
	${}^0L^{\kappa}_{Mo,Ni:Ta}$	−100804	
$D0_a$-I	${}^0L^{D0_a}_{Mo,Ni:Ni:Mo}$	−69324	[8]
	${}^0L^{D0_a}_{Ni:Ni:Mo,Ta}$	$-208456 + 127.928T$	Present
$D0_a$-II	${}^0L^{D0_aII}_{Mo,Ni:Mo}$	−26840	[8]
	${}^0L^{D0_aII}_{Ni:Mo,Ni}$	$4792 - 1.604T$	[8]
	${}^0L^{D0_aII}_{Ni:Mo,Ta}$	${}^0L^{D0_a}_{Ni:Ni:Mo,Ta}/2$	Present
ζ	${}^0L^{\zeta}_{Ni:Mo,Ta}$	−17802	Present
δ	${}^0L^{\delta}_{Ni:Mo,Ni:Mo}$	$-829211 + 825.923T$	[8]
	${}^1L^{\delta}_{Ni:Mo,Ni:Mo}$	$-417368.2 + 326.504T$	

The enthalpy of formation ΔH_f^{Φ} for a given compound Φ is calculated as the difference between the energy E_{TOT}^{Φ} of the compound and linear combination of the pure element reference state energies, E_{Ni}^{fcc}, E_{Mo}^{bcc} and E_{Ta}^{bcc},

$$\Delta H_f^{\Phi} = E_{TOT}^{\Phi} - x_{Ni}^{\Phi}E_{Ni}^{fcc} - x_{Ta}^{\Phi}E_{Ta}^{bcc} - x_{Mo}^{\Phi}E_{Mo}^{bcc} \quad (2)$$

where x_i^{Φ} is the mole fraction of component i in Φ. The calculated enthalpies of formation are plotted in Fig. 2 and listed in Table 6.

The first principles calculations yielded two important results, both shown in Fig. 2. First, it was found that μ-NiTa is not stable at 0 K relative to the compounds C16-$NiTa_2$ and $C11_b$-Ni_2Ta. Second, the compound $D0_{22}$-Ni_3Ta was found to be stable at 0 K with respect to κ-Ni_3Ta, with an energy difference of 6 kJ/mole (atoms). In contrast, the experimental data [6,7,10–12,15,16] in Fig. 1 show that the compound κ-Ni_3Ta is stable at high temperatures. Without specific experimental data indicating the exact temperature of the transition, we assume a temperature of 600 K for the transition from the high temperature stable compound κ-Ni_3Ta (i.e.κ-Ni_3(Mo, Ta) [6,7,10–12,15,16] to the low temperature stable $D0_{22}$-Ni_3Ta phase.

The parameter evaluation process for the Ni–Ta system is started with the liquid phase followed by κ-Ni_3Ta, fcc and bcc and the compounds, ζ-Ni_8Ta, $C11_b$-Ni_2Ta, C16-$NiTa_2$ and μ-NiTa. Due to the significant difference between the experimental data by Sudavtsova [19] and Schaeffers [20], shown in Fig. 3, two sets of parameters for the liquid phase are determined. To select the

Table 6
A summary of results from the first-principles calculations.

Phase	Symbol	Prototype	Formula	ΔH, (kJ/mol)
Ni	A1	fcc	Ni	0
	A2	bcc	Ni	9.33
Mo	A2	bcc	Mo	0
	A1	fcc	Mo	39.51
Ta	A1	fcc	Ta	26.23
	A2	bcc	Ta	0
$Ni_{0.25}Ta_{0.75}$[a]	A2	bcc-SQS16	$Ni_{0.25}Ta_{0.75}$	0.588
$Ni_{0.50}Ta_{0.50}$[a]			$Ni_{0.50}Ta_{0.50}$	−0.23
$Ni_{0.75}Ta_{0.25}$[a]			$Ni_{0.75}Ta_{0.25}$	−5.17
$Ni_{0.25}Ta_{0.75}$[b]	A1	fcc-SQS16	$Ni_{0.25}Ta_{0.75}$	−12.16
$Ni_{0.50}Ta_{0.50}$[b]			$Ni_{0.50}Ta_{0.50}$	−7.54
$Ni_{0.75}Ta_{0.25}$[b]			$Ni_{0.75}Ta_{0.25}$	−9.28
$NiTa_2$	C16	Al_2Cu [33]	Ni_1Ni_2	26.77
			Ta_1Ni_2	44.14
			Ni_1Ta_2	−21.15
			Ta_1Ta_2	50.88
NiTa	μ	Fe_7W_6 [33]	$NiTa_4Ni_2Ni_6$	−12.92
			$TaTa_4Ni_2Ni_6$	−18.61
			$NiTa_4Ta_2Ni_6$	−22.99
			$TaTa_4Ta_2Ni_6$	−25.51
			$TaTa_4Ta_2Ta_6$	17.05
			$TaTa_4Mo_2Ni_6$	−17.52
Ni_2Ta	$C11_b$	$MoSi_2$ [26]	Ni_2Ni	7.91
			Ni_2Ta	−32.36
			Ta_2Ni	5.00
			Ta_2Ta	10.49
NiMo	δ	NiMo	$Ni_{24}Ta_{20}Mo_{12}$	−16.79
			$Ni_{24}Mo_{20}Ta_{12}$	−10.08
			$Ni_{24}Ni_{20}Ta_{12}$	−16.48
			$Ni_{24}Ta_{20}Ta_{12}$	0.62
Ni_3Ta	κ	Pt_3Ta [26]	Ni_3 Ni	3.50
			Ni_3Ta	−29.29
			Ta_3Ni	12.54
			Ta_3Ta	29.32
			Ta_3Mo	32.08
			Mo_3Ta	36.6
			Mo_3Mo	41.09
			Ni_3Mo	−1.86
			Mo_3Ni	18.85
	$D0_a$	Cu_3Ti [26]	Ni_3Ta	−34.81
			Ta_3Ni	12.48
			Ta_3Ta	30.80
	$D0_{22}$	Al_3Ti [26]	Ni_3Ta	−35.29
Ni_8Ta	ζ	Nb_8Ni [14]	Ni_8Ta	−16.37

[a] Reference states: Ni-bcc and Ta-bcc.
[b] Reference states: Ni-fcc and Ta-fcc.

more appropriate parameter set, the parameters for κ-Ni_3(Mo, Ta) are evaluated next. The reason is that the parameters, $a^{\kappa}_{Ni:Ta}$and $b^{\kappa}_{Ni:Ta}$, are fixed with the first-principles data and the melting temperature of κ-Ni_3(Mo, Ta), while the phase equilibrium data liq/liq + κ-Ni_3(Mo, Ta) [10–13] are used to examine the reliability of the liquid parameters. The results indicate that the parameters evaluated from the data by Sudavtsova [19] better reproduce the liquidus for κ-Ni_3(Mo, Ta) [10–13] than do those from the data by Schaefers [20], and the Sudavtsova data [19] are selected for use in the current model description. In addition to $a^{\kappa}_{Ni:Ta}$ and $b^{\kappa}_{Ni:Ta}$, the parameters $a^{\kappa}_{i:j}$ and ${}^0L^{\kappa}$ for κ-Ni_3(Mo, Ta) are evaluated with the first-principles results and reported phase diagram data [6,7,10–13,15].

The enthalpies of mixing for the bcc and fcc solution phases are calculated using three 16-atom SQS [23,24,41] for compositions of

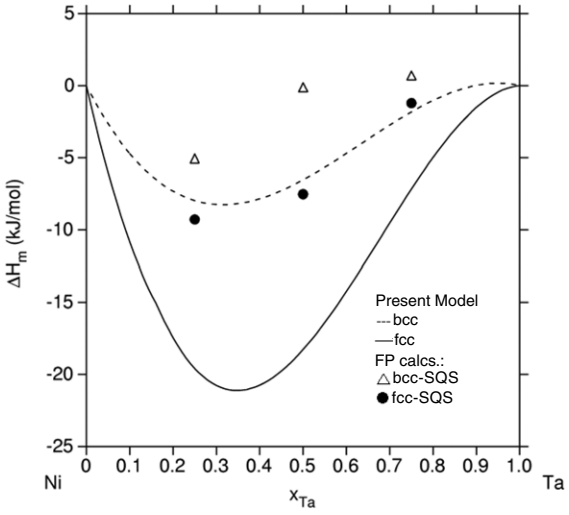

Fig. 4. The enthalpy of mixing, as computed using the present model,for the bcc solution (referenced to bcc-Ni and bcc-Ta) and fcc solution (referenced to fcc-Ni and fcc-Ta).

x_{Ni} = 0.25, 0.5, and 0.75, respectively. Using the same arguments as that for the unstable end-members of the multi-sublattice models, we only relax the cell volume of the SQS without local lattice relaxations. The calculated enthalpies of mixing of the SQS for both bcc and fcc are listed in Table 6 and plotted in Fig. 4. To evaluate the parameters for the fcc and bcc solutions, both the phase equilibrium data [6,7,10,12–16] and the first-principles calculated enthalpies of mixing in Table 6 are considered. Similar to the procedure described above for the liquid and κ-Ni_3(Mo, Ta) phases, the parameters $a^{\zeta}_{Ni:Ta}$ and $b^{\zeta}_{Ni:Ta}$for ζ-Ni_8(Mo, Ta) are determined using the first-principles results and the congruent phase transformation temperature of ζ-Ni_8Ta [15,16], and the experimental data for the fcc/fcc + ζ-Ni_8Ta solvus [6,7,12,13] are subsequently used to determine the fcc parameters.

The parameters $a^{C11_b}_{i:j}$, $a^{D0_{22}}_{Ni:Ta}$, $a^{C16}_{i:j}$, $a^{\mu}_{i:Ta:j:Ni}$ and $a^{\mu}_{Ta:Ta:Ta:Ta}$ are fixed by the first-principles data and the experimental enthalpy of formation [22], as shown in Fig. 2. The parameters $b^{C11_b}_{Ni:Ta}$, $b^{C16}_{Ni:Ta}$ and $b^{\mu}_{Ta:Ta:Ta:Ni}$ and interaction parameters ${}^0L^{C11_b}$, ${}^0L^{C16}_{Ni:Ni,Ta}$, ${}^0L^{C16}_{Ni,Ta:Ta}$, ${}^0L^{\mu}_{Ta:Ta:Ni,Ta:Ni}$ and ${}^0L^{\mu}_{Ta:Ta:Ta:Ni,Ta}$ are evaluated with the phase equilibrium data [6,7,10–12,15]. The parameter $b^{D0_{22}}_{Ni:Ta}$ is evaluated by assuming that the phase transformation κ-Ni_3Ta → $D0_{22}$-Ni_3Ta occurs at 600 K, which can be modified when experimental data become available. The practice is iterative and culminates with an optimized fit involving all available data and calculation results. The overall optimization results are summarized in Tables 4 and 5.

For the Ni–Mo–Ta ternary system, the models for the binary Ni–Ta system described above are combined with reported treatments for the Ni–Mo [8] and Mo–Ta [9] systems, summarized in Tables 4 and 5, respectively. The ternary parameters are evaluated in the order of fcc, κ-Ni_3(Mo, Ta), $D0_a$-Ni_3(Mo, Ta), ζ-Ni_8(Mo, Ta), μ-NiTa, and bcc, based on the availability of experimental data.

The solubility of Mo in κ-Ni_3(Mo, Ta) was experimentally determined by Cui et al. [9], Virkar and Raman [27], and Chakravorty and West [28], indicating that Mo dissolves into κ-Ni_3Ta up to 6 at.% Mo at 1173 K. The Gibbs free energy terms, $\Delta G^{\kappa}_{Mo:Mo}$, $\Delta G^{\kappa}_{Ni:Mo}$, $\Delta G^{\kappa}_{Mo:Ni}$, $\Delta G^{\kappa}_{Mo:Ta}$, $\Delta G^{\kappa}_{Ta:Mo}$, and the interaction parameters, ${}^0L^{\kappa}_{Mo,Ni:Mo}$ and ${}^0L^{\kappa}_{Ni:Mo,Ta}$, are used here to extend the single κ-Ni_3Ta composition range toward the Ni–Mo edge. $\Delta G^{\kappa}_{Mo:Mo}$, $\Delta G^{\kappa}_{Ni:Mo}$, $\Delta G^{\kappa}_{Mo:Ni}$, $\Delta G^{\kappa}_{Mo:Ta}$, and $\Delta G^{\kappa}_{Ta:Mo}$ are assumed to be constant and fixed with the first-principles data. The parameters

Table 7
Invariant reactions in the Ni–Ta system.

Reaction	Calculated results			Experimental Results (K)
	This work	[6]	[7]	
liq + bcc → C16-$NiTa_2$	*T*, K	2060	2067	2051	2061 [12]
	x(liq, Ta)	0.551	0.595	0.559	
	x(bcc, Ta)	0.791	0.788	0.799	
	x(C16, Ta)	0.708	0.692	0.711	
liq + C16Ta_2 → μ-NiTa	*T*, K	1842	1842	1851	1844 [10] 1817–1847 [11] 1843 [12]
	x(liq, Ta)	0.471	0.493	0.486	
	x(C16, Ta)	0.679	0.667	0.674	
	x(μ, Ta)	0.574	0.531	0.530	
liq → κ-Ni_3Ta	*T*, K	1805	1810	1824	1814 [10] 1815 [11] 1808 [12]
	x(liq, Ta)	0.25	0.25	0.25	
	x(κ, Ta)	0.25	0.25	0.25	
liq → fcc + κ-Ni_3Ta	*T*, K	1666	1627	1625	1616–1639 [10] 1643 [11] 1633 [12]
	x(liq, Ta)	0.144	0.139	0.153	
	x(fcc, Ta)	0.137	0.113	0.139	
	x(κ, Ta)	0.241	0.230	0.242	
liq + κ-Ni_3Ta → $C11_b$-Ni_2Ta	*T*, K	1678	1676	1662	1618–1664 [10] 1673 [11] 1678 [12]
	x(liq, Ta)	0.366	0.355	0.357	
	x(κ, Ta)	0.253	0.271	0.279	
	x($C11_b$, Ta)	0.344	0.333	0.341	
liq → μ-NiTa + $C11_b$-Ni_2Ta	T,K	1678	1663	1647	1615–1661 [10] 1639 [11] 1634 [12]
	x(liq, Ta)	0.367	0.373	0.381	
	x(μ, Ta)	0.502	0.500	0.504	
	x($C11_b$, Ta)	0.344	0.333	0.349	
fcc → ζ–Ni_8Ta	T,K	1584	1581	1584	1573 [15] 1593 [16]
	x(liq, Ta)	0.111	0.111	0.111	
	x(κ, Ta)	0.111	0.111	0.111	
fcc → κ–Ni_3Ta + ζ–Ni_8Ta	*T*, K	1571	1580	1547	1572 [13]
	x(fcc, Ta)	0.126	0.1114	0.136	
	x(κ, Ta)	0.237	0.231	0.242	
	x(ζ, Ta)	0.111	0.1111	0.111	
κ-Ni_3Ta + $C11_b$-Ni_2Ta → $D0_{22}$-Ni_3Ta	*T*, K	603	–	–	–
	x(κ, Ta)	0.249(9)	–	–	–
	x($D0_{22}$, Ta)	0.25	–	–	–
	x($C11_b$, Ta)	0.329	–	–	–
κ-Ni_3Ta → $D0_{22}$-Ni_3Ta + ζ-Ni_8Ta	*T*, K	600	–	–	–
	x(κ, Ta)	0.244	–	–	–
	x($D0_{22}$, Ta)	0.25	–	–	–
	x(ζ, Ta)	0.111	–	–	–
μ-NiTa → C16-$NiTa_2$ + $C11_b$-Ni_2Ta	*T*, K	474	–	109	–
	x(μ, Ta)	0.526	–	0.504	–
	x(C16, Ta)	0.666	–	0.667	–
	x($C11_b$, Ta)	0.334	–	0.333	–
κ-Ni_3Ta → ζ-Ni_8Ta + $C11_b$-Ni_2Ta	*T*, K	–	231	42	–
	x(κ, Ta)	–	0.25	0.25	–
	x(ζ, Ta)	–	0.111	0.111	–
	x($C11_b$, Ta)	–	0.333	0.333	–

${}^{i}L^{fcc}_{Ni,Mo,Ta}$, $b^{\kappa}_{Ni:Mo}$, $L^{\kappa}_{Mo,Ni:Mo}$, $L^{\kappa}_{Ni:Mo,Ta}$ and $L^{\kappa}_{Ni,Mo:Ta}$ are evaluated with the phase equilibrium data [9,27,28], as listed in Tables 4 and 5.

The parameters for the $D0_a$-Ni_3Mo phase are determined using the same methodology as described above for the κ-Ni_3(Mo, Ta) phase. Selected parameters ($\Delta G^{D0_a}_{Ta:Ni:Ta}$, $\Delta G^{D0_a}_{Ni:Ni:Ta}$, $\Delta G^{D0_aII}_{Ta:Ta}$, $\Delta G^{D0_aII}_{Ni:Ta}$, $\Delta G^{D0_aII}_{Ta:Ni}$, ${}^{0}L^{D0_a}_{Ni:Ni:Mo,Ta}$, ${}^{0}L^{D0_aII}_{Ni:Mo,Ta}$) are utilized to model the experimentally observed solubility of Ta, reported by Chakravorty and West [28]. Accordingly, these parameters are adjusted to extend the $D0_a$-Ni_3Mo composition range toward the Ni–Ta binary. The parameters $\Delta G^{D0_a}_{Ta:Ni:Ta}$, $a^{D0_a}_{Ni:Ni:Ta}$, $\Delta G^{D0_aII}_{Ta:Ta}$, $a^{D0_aII}_{Ni:Ta}$, and $\Delta G^{D0_aII}_{Ta:Ni}$ are considered as constant and fixed with the first-principles data, while $b^{D0_a}_{Ni:Ni:Ta}$, $b^{D0_aII}_{Ni:Ta}$, ${}^{0}L^{D0_a}_{Ni:Ni:Mo,Ta}$ and ${}^{0}L^{D0_aII}_{Ni:Mo,Ta}$ are evaluated with reported phase boundary data for $D0_a$-Ni_3Mo [28]. For the δ-NiMo phase, the parameters $\Delta G^{\delta}_{Ni:Ta:Mo}$, $\Delta G^{\delta}_{Ni:Mo:Ta}$, $\Delta G^{\delta}_{Ni:Ni:Ta}$ and $\Delta G^{\delta}_{Ni:Ta:Ta}$ are evaluated with the first-principles data.

The bcc phase boundary data in the ternary Ni–Mo–Ta system by Cui et al. [9] and Chakravorty and West [28] are used to determine the ternary interaction parameters for the bcc phase. The interaction parameter ${}^{0}L^{\zeta}_{Ni:Mo,Ta}$ for the ζ-Ni_8(Mo, Ta) phase is evaluated with the experimental data for the ζ-Ni_8(Mo, Ta)/ζ-Ni_8(Mo, Ta)+fcc phase boundary [28]. The ternary parameters $\Delta G^{\mu}_{Ta:Ta:Mo:Ni}$ and ${}^{0}L^{\mu}_{Ta:Ta:Mo,Ta:Ni}$ for the μ phase are evaluated with the first-principles data in Table 6 and experimental data [9,27].

4. Modeling results

The Ni–Ta phase diagram yielded by our modeling is shown in Fig. 1 together with previously proposed phase diagrams [6,7] and

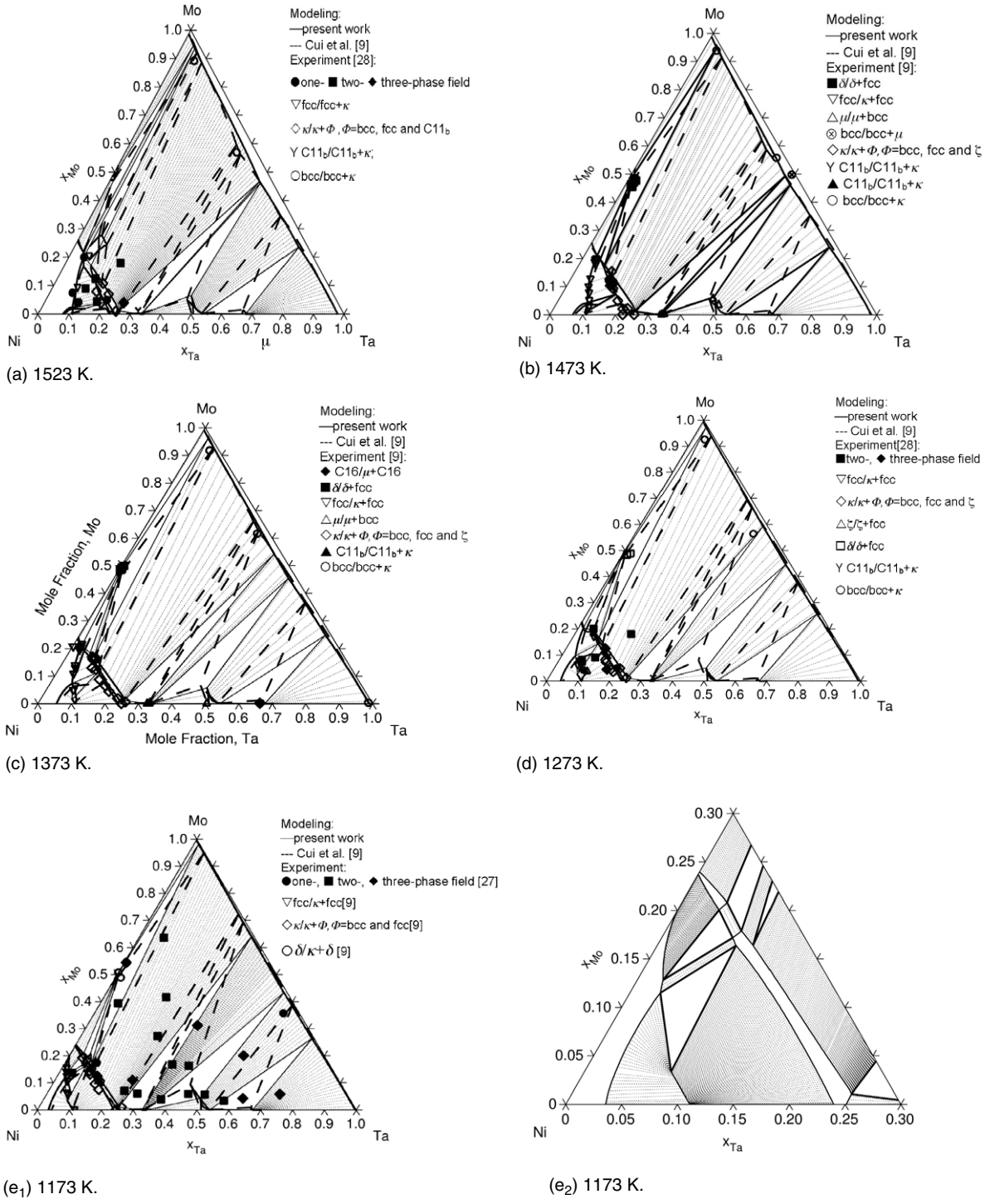

Fig. 5. Isothermal sections of the Ni–Ta–Mo phase diagram, as computed from the present model forthe indicated temperatures. Experimental data are also shown for comparison.

experimental data [6,7,10–16]. The invariant reactions calculated using the parameters in Tables 2, 4 and 5 are summarized in Table 7 and compared with the experimental data [10–13,15,16]. It is shown that the phase diagram in Fig. 1 produced by our model differs significantly from the previous reports [6,7], as highlighted in the following.

The major difference is that we assess the relative low temperature stability of the intermetallic compounds and sublattice end-member phases using first-principles calculations of the zero-Kelvin energies, as described above. Our result shows that the compounds C16-$NiTa_2$, $C11_b$-Ni_2Ta, $D0_{22}$-Ni_3Ta, and ζ-Ni_8Ta in the Ni–Ta system are stable, while the compounds κ-Ni_3Ta and μ-NiTa are not stable at 0 K. The model description of enthalpy of formation is plotted in Fig. 2 and compared with both experimental data and first-principles calculations. It is also shown that the modeling results of Cui and Jin [6] and Pan and Jin [7] are not consistent with the phase stabilities indicated by our first-principles calculations. The enthalpy of mixing for the liquid phase is shown in Fig. 3, and, again, our model provides a better agreement with the experimental data [19] than those reported by Cui and Jin [6] and Pan and Jin [7]. The calculated enthalpies of mixing for the bcc and fcc solutions are plotted in Fig. 4. In comparison with the first-

principles calculations, the model exhibits the appropriate general behavior, though the absolute agreement is rather poor. While this discrepancy, which may be attributed to the relaxation of the cell volume only, is distinct, the first-principles calculation for SQS is a useful option for quantifying the energetics of a solution phase at compositions where experimental measurements cannot be performed. Despite the limitations, in combination with other types of experimental data (e.g. phase boundaries), SQS calculations can contribute to the reliable assessment of thermodynamic model parameters.

The isothermal sections of the Ni–Mo–Ta system were calculated for temperatures 1523, 1473, 1373, 1273 and 1173 K, respectively, as shown in Fig. 5 along with the previously reported results [9] and the experimental data [9,27,28]. The results show that our modeling results differ significantly from the previous reports [9]. The calculated single κ-phase range shows significant difference between our result and that by Cui et al. [9] in Fig. 5, where our results are in good agreement with the experimental data [9,28]. In Fig. 5(a), the calculated isothermal section using the parameters by Cui et al. [9] shows the existence of the liquid phase on Ni-rich corner at 1523 K, while the experimental results by Chakravorty and West [28] did not show the liquid phase on Ni-rich corner. The other significant difference is shown in Fig. 5(e), where the stable $D0_a$-Ni_3Mo and κ-Ni_3Ta phases are treated as two different phases in this work, while Cui et al. [9] treat them as the same phase. Our treatment, thus, provides a basis for extending the model to other systems or subsystems with the $D0_a$ (Cu_3Ti structure) and/or κ (Pt_3Ta structure) phases. In Fig. 5(e), our results show good agreement with the experimental data [9,27]. The third significant difference between our modeling and that of Ref. [9] is the direction of the tie-lines from the Ni-rich part towards Mo–Ta side of the system. This difference results from the Ni–Ta and Ni–Mo binaries, in which the first-principles results were employed in our modeling to determine the model parameters for both compound and solid solution phases. Fig. 2 and the figures in Ref. [8] show the calculated enthalpy of formation in which the difference between our model and that of Ref. [9] can be identified. Considering the experimental data for bcc/bcc + κ in Fig. 5(b) and (d), our results are reasonable, while those calculated bcc + κ two-phase field by Ref. [9] deviates from the experimental data [9,28]. To understand the stability of the fcc phase, we plotted the stable fcc phase field in the related composition triangle over a range of temperature in Fig. 6, which is useful for Ni-base superalloy design by showing the stable γ-fcc phase domain with related composition and temperature dimensions. To see the temperature dependent liquidus surface, we plot the liquidus projection for the Ni–Mo–Ta system along with the experimental data [28] in Fig. 7.

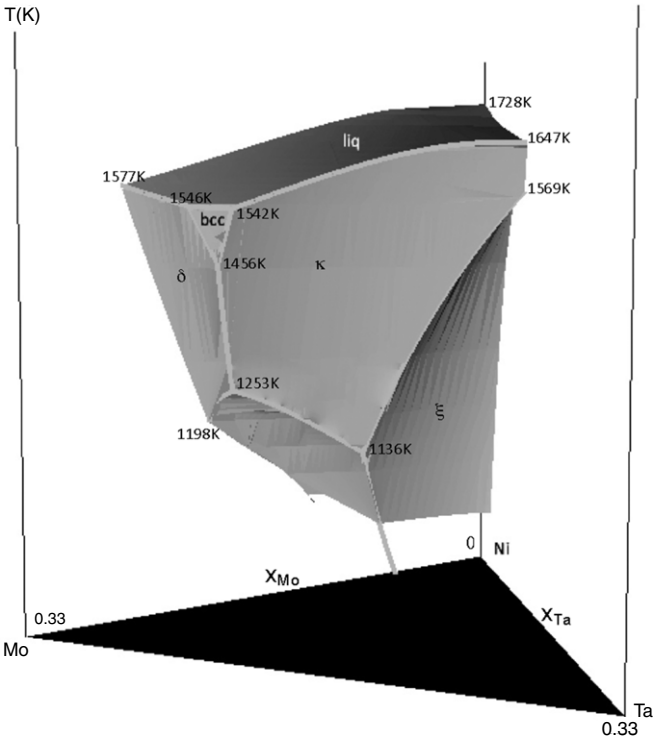

Fig. 6. The fcc single-phase field, as computed using the present model.

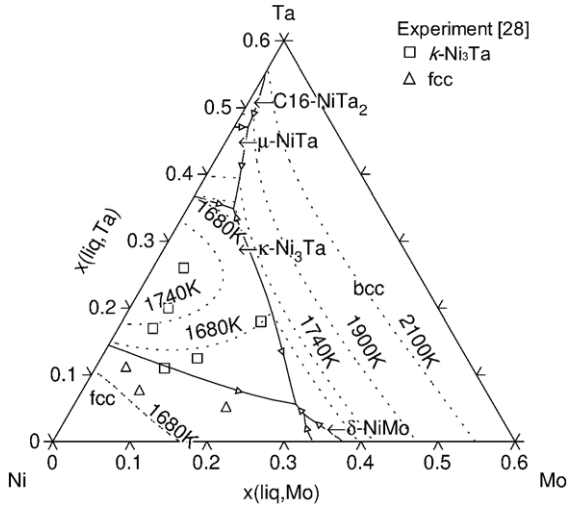

Fig. 7. The liquidus composition-plane projection indicating the primary phases and comparing with experimental data [28] for the Ni–Mo–Ta system, as computed using the current model.

5. Summary and conclusions

By combining a CALPHAD approach and first-principles calculations, the Gibbs free energy functions of individual phases in the binary Ni–Ta and ternary Ni–Mo–Ta systems are evaluated, and the associated equilibrium phase diagrams are reported. The present work exhibits several key differences from previously reported thermodynamic modeling, which are that (i) the first-principles calculated enthalpies of formation indicate that the compound $D0_{22}$-Ni_3Ta is stable while κ-Ni_3Ta and μ-NiTa are metastable at 0 K, (ii) the phase boundaries in the binary Ni–Ta system are in better agreement with experimental observations, (iii) the calculated phase diagrams for the Ni–Mo–Ta system show good agreement with the experimental data.

Acknowledgements

Work performed within the Ames Laboratory was supported by the Department of Energy-Basic Energy Sciences under Contract no DE-AC02-07CH11358. First-principles calculations were carried out on the LION clusters at the Pennsylvania State University supported in part by the NSF grants (DMR-9983532, DMR-0122638, and DMR-0205232) and in part by the Materials Simulation Center and the Graduate Education and Research Services at the Pennsylvania State University.

Appendix. Supplementary data

Supplementary data associated with this article can be found, in the online version, at doi:10.1016/j.calphad.2009.06.006.

References

[1] N. Dupin, I. Ansara, B. Sundman, CALPHAD 25 (2001) 279–298.
[2] I. Ansara, N. Dupin, H.L. Lukas, B. Sundman, J. Alloys. Compd. 247 (1997) 20–30.
[3] S.H. Zhou, Y. Wang, J.Z. Zhu, T. Wang, L.Q. Chen, R.A. MacKay, Z.K. Liu, Integration of computational tools for designing ni-base superalloys, in: R.C. Reed (Ed.), Superalloys, 2004, pp. 969–976.
[4] L. Kaufman, CALPHAD 15 (1991) 243–259.
[5] I. Ansara, M. Selleby, CALPHAD 18 (1994) 99–107.
[6] Y.W. Cui, Z.P. Jin, Z. Metak. 90 (1999) 233–241.
[7] X.M. Pan, Z.P. Jin, Trans. Nonferr. Met. Soc. China 12 (2002) 748–753.
[8] S.H. Zhou, Y. Wang, C. Jiang, J.Z. Zhu, L.-Q. Chen, Z.-K. Liu, Mater. Sci. Eng. A 397 (2005) 288–296.
[9] Y.W. Cui, X.G. Lu, J.P. Jin, Metall. Mater. Trans. A 30 (1999) 2735–2744.
[10] E. Therkelsen, Met. Alloys 4 (1933) 105–108.
[11] O. Kubaschewski, H. Speidel, J. Inst. Met. 75 (1949) 417–420.
[12] I.I. Kornilov, E.N. Plyaeva, Russ. J. Inorg. Chem. 7 (1962) 300–303.
[13] I.I. Kornilov, E.N. Pylaeva, Dokl. Akad. Nauk SSSR 91 (1953) 841–843.
[14] J.M. Larson, R. Taggart, D.H. Polonis, Metell. Trans. 1 (1970) 485–489.
[15] V.N. Pimenov, Y.U.E. Ugaste, K.A. Akkushkarova, Russ. Metall. (1977) 155–159.
[16] P. Nash, D.R.F. West, Met. Sci. 17 (1983) 99–100.
[17] L. Kaufmann, H. Bernstein, Computer Calculation of Phase Diagrams, Academic Press, Inc., New York, 1970.
[18] N. Saunders, A.P. Miodownik, CALPHAD (Calculation of Phase Diagrams): A Comprehensive Guide, Pergamon, Oxford, New York, 1998.
[19] V.S. Sudavtsova, Russ. Metall. (1998) 54–56.
[20] K. Schaeffers, J. Qin, M. Rosner-Kuhm, M.G. Frohberg, Can. Metall. Q. 35 (1996) 47–51.
[21] N.P. Lyakishev, Y.U.P. Snitko, V.I. Alekseev, G.A. Levshin, Dokl. Akad. Nauk SSSR 258 (1981) 1404–1406.
[22] F. Sommer, J. Schott, B. Predel, Z. Met.kd. 76 (1985) 369–371.
[23] C. Jiang, C. Wolverton, J. Sofo, L.-Q. Chen, Z.-K. Liu, Phys. Rev. B 69 (2004) 214202.
[24] A. Zunger, S.H. Wei, L.G. Ferreira, J.E. Bernard, Phys. Rev. Lett. 65 (1990) 353–356.
[25] R.E.W. Casselton, W. Hume-Rothery, J. Less-Common Met. 7 (1964) 212–221.
[26] B.C. Giessen, N.J. Grant, Acta Metall. 15 (1967) 871–877.
[27] A.V. Virkar, A. Raman, Z. Met.kd. 60 (1969) 594–600.
[28] S. Chakravorty, D.R.F. West, Met. Sci. 17 (1983) 573–580.
[29] S. Chakravorty, D.R.F. West, J. Mater. Sci. Lett. 2 (1983) 583–586.
[30] A.T. Dinsdale, CALPHAD 4 (1991) 317–425.
[31] B. Sundman, J. Agren, J. Phys. Chem Solids 42 (1981) 297–301.
[32] O. Redlich, A.T. Kister, Ind. Eng. Chem. 40 (1948) 345–348.
[33] P.I. Kripyakevich, E.I. Gladyshevskii, E.N. Pylaeva, Soviet. Phys. Crystallogr. 7 (1962) 165–168.
[34] S.K. Das, G. Thomas, Phys. Status Solidi 21 (1974) 177–190.
[35] J.O. Andersson, A.F. Guillermet, M. Hillert, B. Jansson, B. Sundman, Acta Metall. 34 (1986) 437–445.
[36] I. Ansara, T.G. Chart, A.F. Guillermet, F.H. Hayes, U.R. Kattner, D.G. Pettifor, N. Saunders, K. Zeng, CALPHAD 21 (1997) 171–218.
[37] J.M. Joubert, N. Dupin, Intermetallics 12 (2004) 1373–1380.
[38] G. Kresse, T. Demuth, F. Mittendorfer, VAMP/VASP, 2003 http://cms.mpi.univie.ac.at/vasp/.
[39] D. Vanderbilt, Phys. Rev. B 41 (1990) 7892–7895.
[40] J.P. Perdew, J.A. Chevary, S.H. Vosko, K.A. Jackson, M.R. Pederson, D.J. Singh, C. Fiolhais, Phys. Rev. B 46 (1992) 6671–6687.
[41] S.H. Wei, L.G. Ferreira, J.E. Bernard, A. Zunger, Phys. Rev. B 42 (1990) 9622–9649.